Journal of Power Sources 189 (2009) 552–556

Contents lists available at ScienceDirect

Journal of Power Sources

journal homepage: www.elsevier.com/locate/jpowsour

Short communication

Some new facts on electrochemical reaction mechanism for transition metal oxide electrodes

Chunhua Chen[a,*], Ning Ding[a,b], Long Wang[a], Yan Yu[a], Ingo Lieberwirth[b]

[a] Department of Materials Science and Engineering, University of Science and Technology of China, Anhui Hefei 230026, China
[b] Max Planck Institute for Polymer Research, Mainz 55128, Germany

ARTICLE INFO

Article history:
Received 11 June 2008
Received in revised form 7 October 2008
Accepted 9 October 2008
Available online 1 November 2008

Keywords:
Transition metal oxides
Conversion reaction
Interfacial storage
Lithium-ion batteries

ABSTRACT

Transition metal oxides represent a new type of anode materials for lithium-ion batteries. Due to their high capacity (usually above 700 mAh g^{-1}) and excellent cycleability, they have attracted much attention in recent years. Regarding the electrochemical reaction mechanism for this type of electrode, the conversion reaction mechanism proposed by Tarascon and co-workers is widely accepted, i.e. $MO_x + 2xLi \leftrightarrows M + xLi_2O$. Nevertheless, in our recent explorations, we have found some new phenomena which may help us to further understand the electrode reaction mechanism, and even pose a necessity to modify the current conversion reaction mechanism. These new phenomena can be summarized as electrochemical milling, capacity rise and no-metal-formation effects.

1. Introduction

Some transition metal oxides (FeO, CoO, NiO, CuO and so on) can reversibly react with lithium in lithium batteries and might be used as anode materials for lithium-ion batteries [1–6]. These transition metal oxides usually exhibit a large rechargeable capacity; for example, the capacity of CoO can reach 700 mAh g^{-1}, more than twice of that for graphite, which is widely used in commercial batteries [7–9]. In addition, these materials also show an excellent cycleability; they can be cycled for hundreds of times with little capacity fading [10,11]. For comparison, silicon, which is another anode material, also has a very high capacity, but its cycleability is very poor due to the volume inflation during lithium intercalation [12,13]. Therefore, transition metal oxides are the potential candidates for high energy lithium-ion batteries.

Different from the classic intercalation materials, such as $LiCoO_2$, these oxides have no suitable vacancies in their crystal lattices to store lithium ions. Tarascon's group [1] has demonstrated by X-ray and electron diffraction that this material undergoes a so-called conversion reaction and forms metal/Li_2O nanocomposites. Their study was first published in *Nature* in 2000, and up to now, this conversion mechanism has been widely accepted [14–17]. Recently, in our own explorations, some new phenomena have been found, which may help us to further understand the electrode reaction process, and even pose a necessity to modify the current conversion reaction mechanism. These new phenomena can be summarized as electrochemical milling, capacity rise and no-metal-formation effects. In this paper, we present the relevant experimental results and discussion and hope to stimulate investigations on this kind of exciting anode material.

2. Experimental

The transition metal oxide electrodes were respectively made into a laminate form by tape-casting method, a thin-film form by electrostatic spray deposition (ESD) and a nanofiber form by electrospinning method.

A slurry consisting of 40 wt% MnO_2 (from Merck, 90%), 30 wt% polyvinylidene fluoride (PVDF) and 30 wt% carbon black was cast on a copper foil and was dried in the dry box to make anodes for 2032 coin cells. The cells were assembled in an argon-filled glove box with Li sheets as counter electrode and 1 mol $LiPF_6$ solution in 1:1 ethylene carbonate:diethyl carbonate as the electrolyte. The cells were cycled on a multi-channel battery test system (NEWARE BTS-610) between 0 and 3 V at a constant current density of 0.2 mA cm^{-2}.

Thin films of Cu–Li–O (Cu:Li = 1:1) composite electrodes supported on nickel foam and copper foil substrate were prepared under optimized conditions at 250 °C by the well-established electrostatic spray deposition technique. The precursor solution was made by dissolving copper acetate and lithium acetate in butyl car-

* Corresponding author. Tel.: +86 551 3606971; fax: +86 551 3601592.
E-mail address: cchchen@ustc.edu.cn (C. Chen).

0378-7753/$ – see front matter © 2008 Elsevier B.V. All rights reserved.
doi:10.1016/j.jpowsour.2008.10.052

bitol. A distance of 4–5 cm was kept between the needle and the substrate. The applied voltage was 10–18 kV.

A typical electrospinning method was adopted to fabricate carbon fiber or C/Fe_3O_4 fibers. Polyacrylonitrile (PAN) (M.W. ~ 86,000) was dissolved in *N*-*N*-dimethylformamide (DMF) to form a polymer precursor, which was used to prepare carbon nanofiber. Also, ferric acetylacetonate ($Fe(acac)_2$) was added into the polymer solution as a precursor for electrospinning of C/Fe_3O_4 fibers. The electrospun fibers were pre-oxidized at 240 °C in air for 6 h. Then, pure carbon and C/Fe_3O_4 composite nanofibers were obtained by a subsequent annealing (carbonization) at 600 °C in argon for 10 h. Finally, the carbon-based nanofibers were cast on a copper foil with a PVDF binder to prepare the electrodes. The weight ratio of the active materials and the binder was controlled as 10:1.

The morphology of thin films and fibers was examined with a scanning electron microscope (SEM, Hitachi X-650 and LEO 1530 Gemini). Electron energy loss spectra (EELS) were recorded from a Zeiss 912 microscope operated at 120 kV with an in-column Omega energy filter. Energy loss was calibrated before measurement using a standard NiO_x sample to the peak of Ni–L_3 edge at 854 eV. All spectra were recorded using a parallel-mode with a spectral magnification of 163×. The energy resolution was about 1.8 eV with an energy dispersion of 0.12 eV $pixel^{-1}$. TEM images and selected area electron diffraction (SAED) patterns were obtained from Tecnai F20 operating at 200 kV. The cells for EELS and TEM were disassembled in an argon-filled glove box. The electrodes were washed with anhydrous dimethyl carbonate (DMC) to remove the electrolyte residues. The samples were milled in 1-methyl-2-pyrrolidone (NMP) and dropped on holey carbon grids. The grids were immediately transferred to electron microscope after being taken outside from the glove box (less than 5 min).

3. Results and discussion

3.1. Electrochemical milling effect

The most interesting phenomenon of transition metal oxides working as the anode materials for lithium-ion batteries is the electrochemical milling effect. After lithiation, the bulk particles of the electrode can be degraded into nanoparticles. To make this powderization process more distinct, the nanofibers of pure carbon and C/Fe_3O_4 composite were obtained successfully via an electrospinning method followed with a subsequent carbonization process (Fig. 1a) [18]. The electrospun nanofibers of pure carbon and C/Fe_3O_4 composite behave differently after electrochemical cycling: the pure carbon retains its morphology (Fig. 1b), whereas the composite containing Fe_3O_4 becomes powderized (Fig. 1c). Such a powderization or electrochemical milling effect has also been found in other studies when a transition metal oxide is used as the anode. In our previous study [19], we have found that the powderization process and the morphology of final products are associated with the cycling temperature. Thus, it is believed that the small diffusion coefficient of lithium in metal and Li_2O can be accounted to understand this effect. To avoid the difficult diffusion of lithium within the electrode grains, fracture of the electrode takes place in most of the grains which turns finally into the powderization of the electrode. Once the powderization appears, lithium ions can diffuse fast along the cracks to the surface of the metal oxide particle. In the case of C/Fe_3O_4, such a powderization effect is more severe because the presence of carbon (C) results in a denser morphology of the electrode fiber (Fig. 1a).

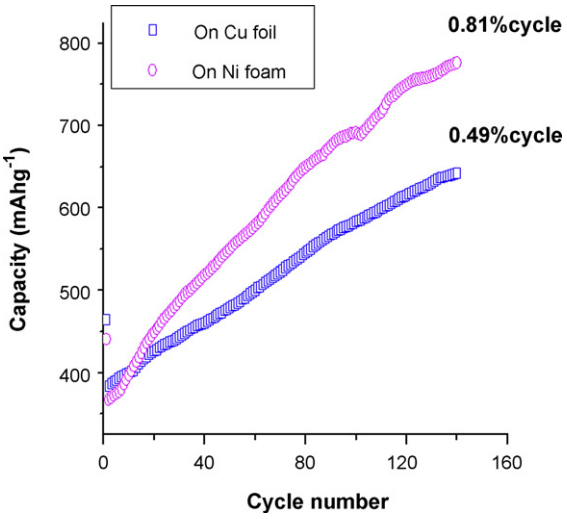

Fig. 2. Electrochemical performance of Cu_2O–Li_2O (Li:Cu = 1:1) thin-film electrodes cycled between 0.01 and 3 V vs. Li^+/Li: voltage profiles. The current density was 0.1 mA cm^{-2} (about 1 C).

3.2. Capacity rise effect

The other interesting phenomenon is the capacity of transition metal oxides rise with cycling, which is very rarely observed in the electrodes made of intercalation compounds such as $LiCoO_2$, $LiMn_2O_4$ and $Li_4Ti_5O_{12}$. According to the proposition of Tarascon's group, a gel-like film, coming from the decomposition of the electrolyte at the low voltage, plays a crucial role in the capacity rise [11]. In our case of Cu_2O–Li_2O (Li:Cu = 1:1) thin-film electrode, it has been also observed that its capacity rises with cycling (Fig. 2), as fast as 0.81% per cycle, much faster than that in any other reports [20,21]. In other words, after 120 cycles, its capacity can even reach

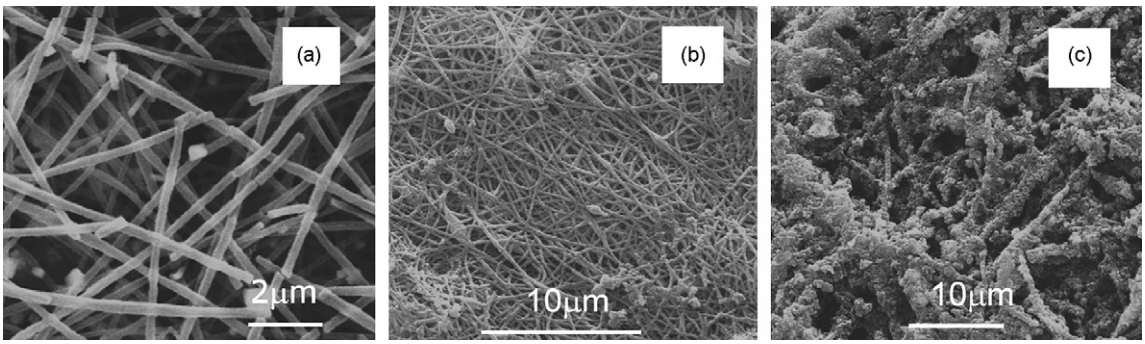

Fig. 1. SEM of C/Fe_3O_4 nanofiber before cycling (a) and electrodes after 80 cycles: carbon nanofiber (b) and C/Fe_3O_4 nanofiber (c).

twice of that in the first several cycles. By examining the electronic structure of Cu_2O–Li_2O after 50 cycles (charged to 3 V), the existence of Cu(II) is detected, suggesting that Li_2O can work as an oxidant and participate into the cycling as the following reaction: $Cu_2O + Li_2O \leftrightarrows 2CuO + 2Li$. Similar phenomenon has also been found in the CoO–Li_2O composite electrode, which has been reported by our group previously [8].

3.3. No-metal-formation fact

In fact, the two aspects (electrochemical milling effect and capacity rise effect) mentioned above have been reported by us and other groups before. The main point in this paper is to introduce another phenomenon, where the transition metal oxide does not follow the conversion reaction mechanism to form elemental metal. One example is β-MnO_2. Fig. 3a is the SEM image of β-MnO_2 and the inset is its X-ray diffraction pattern (space group: $P4_2/mnm$), which is different from the γ-MnO_2 used in primary MnO_2/Li battery [22]. The charge–discharge voltage profile of β-MnO_2 is shown in Fig. 3b. Two plateaus, at 0.65 and 0.29 V, are observed in the first discharge process. The first plateau at 0.65 V is related to the lithium intercalation into carbon black, which is added to enhance the electronic conductivity when preparing the electrode, and according to the study of Takei et al., this plateau is irreversible and can only be observed in the first cycle [23]. Following the first plateau associated with carbon black, there is a long and quite flat plateau at 0.29 V, which should come from the reaction(s) between lithium and β-MnO_2. By subtracting the capacity from carbon black, there is about 4 mol Li reacting with β-MnO_2, which seems to completely reduce MnO_2 to Mn, just following the conversion mechanism. However, the plateau at 0.29 V is much lower than the theoretical calculation result of the reduction plateau (at 1.703 V, according to the Gibbs energy change of the reaction: $MnO_2 + 4Li \leftrightarrows Mn + 2Li_2O$). Moreover, by means of EEL spectra, we examined the electronic structures of β-MnO_2 at different charge–discharge states. Surprisingly, the results quite conflict with the conversion mechanism. Fig. 3c shows the EEL spectra of Mn L-edge for β-MnO_2 discharged to 0 V and some reference manganese oxides (Mn, MnO, Mn_2O_3, $LiMn_2O_4$ and β-MnO_2). In comparison with the energy loss of EEL spectra for reference samples with different valence states of Mn, the valence of Mn in the full-lithiated β-MnO_2 is between +2 and +3. Astonishingly, this EELS result implies that β-MnO_2 is only partially reduced, even after the apparent full lithiation, corresponding to 4 mol Li reacting with β-MnO_2. Obviously, this phenomenon cannot be explained by the traditional conversion mechanism. Nonetheless, the phenomenon of partial reduction of transition metal oxides, even after reacting with a large amount of lithium, which is enough to totally reduce the oxides to metal, is not unique. Similar phenomena have also been reported in $MnMoO_4$ and MnV_2O_7 systems [24,25], where the valence of Mn changes from +4 to +2, and the valence of V changes from +5 to +3 after full lithiation, corresponding to forming $Li_{12}MnV_2O_7$ compound. For there are only two valence states of Li (0 and +1), to achieve the valence balance, Piffard et al. [24] proposed that only 50% charge of Li can transfer to MnV_2O_7. Besides the transition metal oxides, vanadium diphosphide (VP_2), whose electronic structure has not even changed during lithiation, was also reported by Gillot et al. recently [26].

To determine the final structure of β-MnO_2 after full lithiation, TEM and SAED analyses were carried out and the TEM image and SAED pattern are shown in Fig. 4. After being discharged, the bulk β-MnO_2 particles are degraded into nanoparticles, with a diameter of about 5 nm, which also confirms the electrochemical milling effect on β-MnO_2. By indexing the SAED pattern (the inset), the

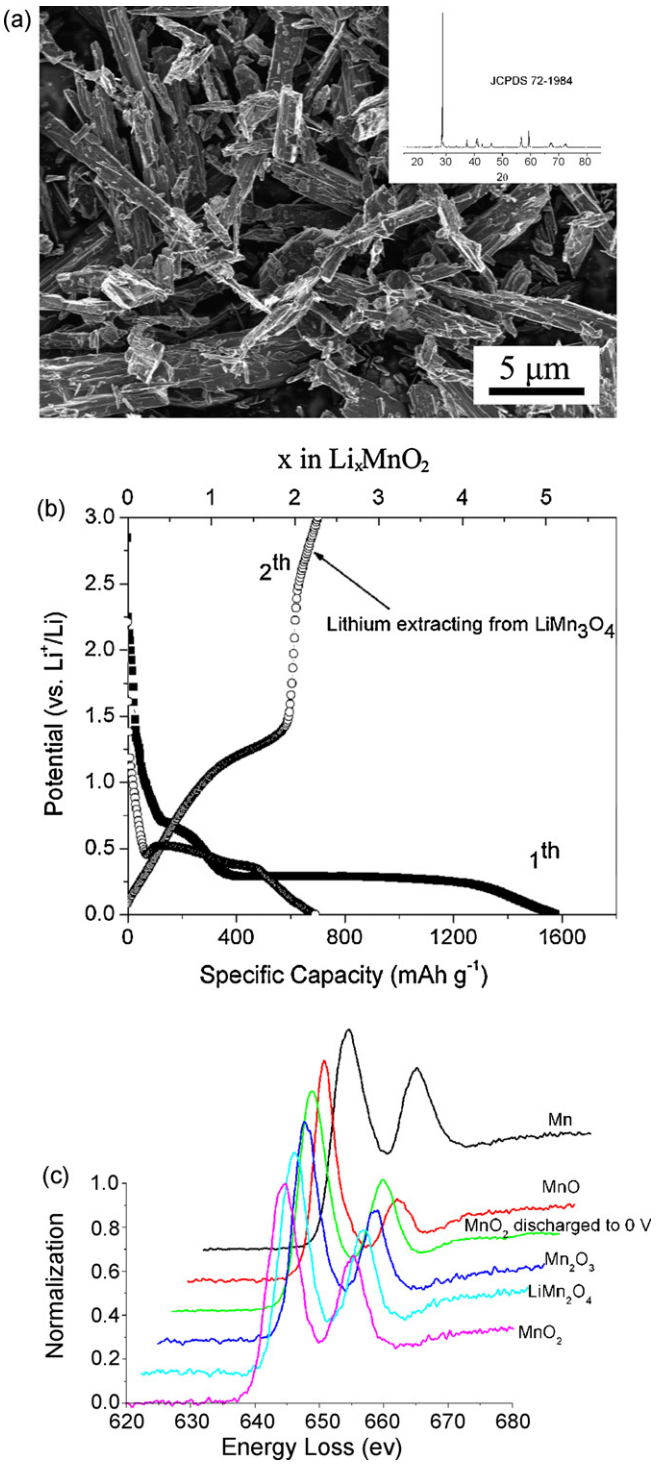

Fig. 3. (a) SEM image of β-MnO_2 and its XRD pattern (the inset); (b) the charge–discharge voltage profile of β-MnO_2/Li cells; (c) EEL spectra of Mn L-edge for full-lithiated β-MnO_2 (to 0 V) and the reference manganese oxides with difference valence states.

final composition of full-discharged β-MnO_2 is $LiMn_3O_4$ with lattice constants $a = 6.022$ and $c = 9.011$ Å (space group: $I4_1/amd$, JCPDS 38-0298). For the first strongest diffraction dot from (0 1 1) facet, as indexed in Fig. 4 inset, is with a large distance ($d_{(011)} = 5.007$ Å), it is easy to differentiate $LiMn_3O_4$ from other manganese oxides or even Mn. For example, the distances of the first strongest diffraction dots of β-MnO_2 ($P4_2/mnm$), Mn_2O_3 (Ia3), MnO (Fm3-m)

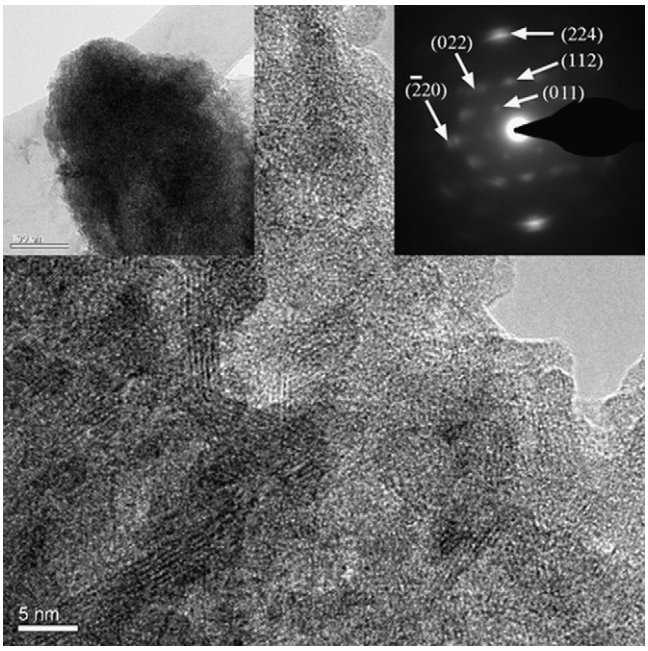

Fig. 4. TEM image and SAED pattern of full-lithiated β-MnO_2.

and Mn (I4-3m) are 3.114, 2.722, 2.581 and 2.101 Å, respectively. Thus, it is clear that β-MnO_2 undergoes such a reaction during discharge:

$$MnO_2 + \tfrac{5}{3}Li \leftrightarrows \tfrac{1}{3}LiMn_3O_4 + \tfrac{2}{3}Li_2O$$

However, this reaction can only assume 5/3 mol Li, much less than the experimental assumption (4 mol Li). Then, where are the excess lithium sources and how do they exist in lithiated β-MnO_2? Herein, we incline to use the interfacial storage mechanism proposed by Maier's group [27–30]. Nevertheless, somewhat different from the traditional interfacial storage model, where only a small amount of lithium can be stored on the interface (usually less than 1 mol), our model needs the interface to store a large amount (7/3 mol, at this moment we omit the lithium consuming for forming solid-state electrolyte interface). The thickness of the lithium storage on the interface can be simply evaluated using the core–shell model:

$$\frac{7}{3} \times \frac{(4/3)\pi R^3 \times \rho_{LiMn_3O_4}}{M_{LiMn_3O_4}} = \frac{1}{3} \times \frac{[(4/3)\pi(R+r)^3 - (4/3)\pi R^3] \times \rho_{Li}}{M_{Li}}$$

the mole ratio of $LiMn_3O_4$ and interfacial lithium is 1/3 to 7/3, the total reaction should be

$$MnO_2 + 4Li \leftrightarrows \tfrac{1}{3}LiMn_3O_4 + \tfrac{2}{3}Li_2O + \tfrac{7}{3}Li$$

where R is the radius of $LiMn_3O_4$ nanoparticles (assuming 2.5 nm) and r is the thickness of the lithium stored on the interface, whereas $\rho_{(LiMn_3O_4)}$ and $\rho_{(Li)}$ can be calculated according to their cell volumes. The calculation result of r is 0.52 nm. Considering the light atom of lithium and the bombarding effect of electron on lithium, for which even the metallic lithium appears "boiled" during TEM observation at 200 kV [31], it is hard to observe this thin film of interfacial lithium storage. On the other hand, the conversion reaction mechanism is built on that the reduced metal nanoparticles can work as a catalyst to decompose Li_2O in the following charge process. However, in our case, it is hard to believe that $LiMn_3O_4$ can play the

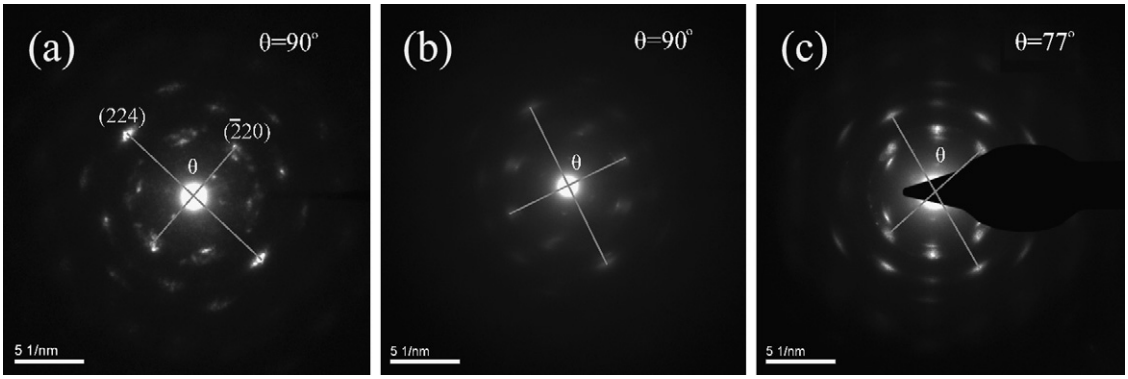

Fig. 5. Comparison of the SAED patterns of (a) full-lithiated β-MnO_2 (to 0 V), (b) partial delithiated β-MnO_2 (to 1.8 V) and (c) full-delithiated β-MnO_2 (to 3 V).

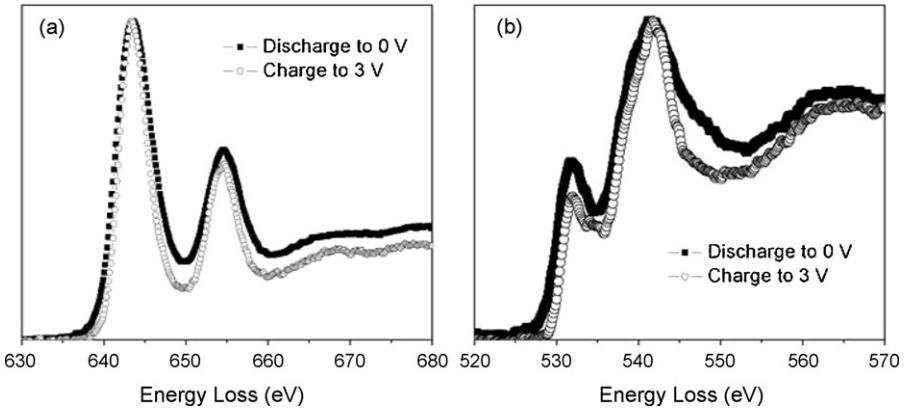

Fig. 6. EEL spectra of (a) Mn L-edge and (b) O K-edge for full-lithiated and full-delithiated β-MnO_2.

same role as those metal nanoparticles. Therefore, it is necessary to study the following charge process of lithiated β-MnO_2.

The SAED patterns of β-MnO_2 at the different charge–discharge states are shown in Fig. 5. During delithiation, the distances of lattice planes are almost without any change (the composition is still $LiMn_3O_4$) and the whole SAED pattern at 1.8 V keeps the same as that at 0 V. Obviously, the conversion reaction mechanism can not explain this phenomenon. Furthermore, the amount of cycling lithium of β-MnO_2 in the charge process (to 1.8 V) is about 2 mol, which is almost equal to the lithium amount storage on the interface (7/3 mol, the slight difference might be due to the formation of solid-state electrolyte interface, which can also consume some lithium source.). Therefore, we propose that the lithium storage on the interface by charge transfer plays a crucial role in the cycling lithium storage. In addition, it is also observed that when the cell is charged to 3 V, the angle between (2 2 4) and (−2 2 0) tilts from 90° to 77°, indicating that the crystal structure of $LiMn_3O_4$ undergoes a monoclinic or triclinic transition. By carefully studying the charge voltage profile of β-MnO_2 (Fig. 3b), we can find that there is a shoulder when the charge voltage is beyond 2 V, probably corresponding to the lithium extraction from $LiMn_3O_4$. The lithium extraction leads to the structure failure of $LiMn_3O_4$, because similar phenomenon is also found in $LiCoO_2$ system, where the crystal structure of $LiCoO_2$ can change from hexagonal to monoclinic when the voltage is beyond 4.2 V [32]. For the amount of lithium extracted from $LiMn_3O_4$ is small, the electronic structures of Mn and O do not show too much difference from those at 0 V, confirmed by the EEL spectra as shown in Fig. 6.

4. Conclusions

We briefly summarizes our recent findings of electrochemical milling and capacity rise effects on the study of transition metal oxides working as the anode materials for lithium-ion batteries, then focus to study the reaction process between β-MnO_2 and lithium in batteries. We astonishingly find that β-MnO_2 is only partially reduced to $LiMn_3O_4$, instead of being reduced to Mn, even after it has reacted with 4 mol Li. Furthermore, by SAED and EELS study, we propose that the lithium storage on the interface of $LiMn_3O_4$ plays a crucial role in the cycling lithium storage. During the lithiation and delithiation, the $LiMn_3O_4$ host exhibits hardly significant change. We anticipate our study can help to further understand the reaction mechanism of transition metal oxides and lithium in batteries.

Acknowledgements

N. Ding thanks the financial support of the doctoral promotion program launched between Chinese Academy of Sciences and Max-Planck-Gesellschaft. The authors thank Prof. Maier (Max Planck Institute for Solid State Research in Stuttgart) for helpful discussion.

Appendix A. Supplementary data

Supplementary data associated with this article can be found, in the online version, at doi:10.1016/j.jpowsour.2008.10.052.

References

[1] P. Poizot, S. Laruelle, S. Grugeon, L. Dupont, J.M. Tarascon, Nature 407 (2000) 496–499.
[2] P.L. Taberna, S. Mitra, P. Poizot, P. Simon, J.-M. Tarascon, Nat. Mater. 5 (2006) 567–573.
[3] Y.-S. Hu, Y.-G. Guo, W. Sigle, S. Hore, P. Balaya, J. Maier, Nat. Mater. 5 (2006) 713–717.
[4] S. Grugeon, S. Larruelle, R. Herrera-Urbina, L. Dupont, P. Poizot, J.-M. Tarascon, J. Electrochem. Soc. 148 (2001) A285–A292.
[5] H. Li, X.J. Huang, L.Q. Chen, Solid State Ionics 123 (1999) 189–197.
[6] P. Balaya, H. Li, L. Kienle, J. Maier, Adv. Funct. Mater. 13 (2003) 621–625.
[7] E. Peled, C. Menachem, D. BarTow, A. Melman, J. Electrochem. Soc. 143 (1996) L4–L7.
[8] Y. Yu, C.-H. Chen, J.-L. Shui, S. Xie, Angew. Chem. Int. Ed. 44 (2005) 7085–7089.
[9] J.-S. Do, C.-H. Weng, J. Power Sources 146 (2005) 482–486.
[10] Y.-M. Kang, M.-S. Song, J.-H. Kim, H.-S. Kim, M.-S. Park, J.-Y. Lee, H.K. Liu, S.X. Dou, Electrochim. Acta 50 (2005) 3667–3673.
[11] S. Laruelle, S. Grugeon, P. Poizot, M. Dollé, L. Dupont, J.-M. Tarascon, J. Electrochem. Soc. 149 (2002) A627–A634.
[12] S.-H. Ng, J.Z. Wang, D. Wexler, K. Konstantinov, Z.-P. Guo, H.-K. Liu, Angew. Chem. Int. Ed. 41 (2006) 6896–6899.
[13] C.K. Chan, H. Peng, G. Liu, K. Mclwrath, X.F. Zhang, R.A. Huggins, Y. Cui, Nat. Nanotechnol. 3 (2008) 31–35.
[14] H.C. Choi, S.Y. Lee, S.B. Kim, M.G. Kim, M.K. Lee, H.J. Shin, J.S. Lee, J. Phys. Chem. B 106 (2002) 9252–9260.
[15] R. Dedryvère, S. Laruelle, S. Grugeon, P. Poizot, D. Gonbeau, J.-M. Tarascon, Chem. Mater. 16 (2004) 1056–1061.
[16] J. Ma, W.-Y. Liu, C.-L. Li, Z.-W. Fu, Electrochim. Acta 51 (2006) 2030–2041.
[17] H.-C. Liu, S.-K. Yen, J. Power Sources 166 (2007) 478–484.
[18] L. Wang, Y. Yu, P.C. Chen, D.W. Zhang, C.H. Chen, J. Power Sources 183 (2008) 717.
[19] D.W. Zhang, C.H. Chen, J. Zhang, F. Ren, Chem. Mater. 17 (2005) 5242–5245.
[20] Y. Yu, Y. Shi, C.H. Chen, Nanotechnology 18 (2007) 055706.
[21] C.Q. Zhang, J.P. Tu, X.H. Huang, Y.F. Yuan, X.T. Chen, F. Mao, J. Alloys Compd. 441 (2007) 52–56.
[22] M.M. Thackeray, Prog. Solid State Chem. 25 (1997) 1–71.
[23] K. Takei, K. Kumai, Y. Kobayashi, H. Miyashiro, T. Iwahori, T. Uwai, H. Ue, J. Power Sources 54 (1995) 171–174.
[24] Y. Piffard, F. Leroux, D. Guyomard, J.-L. Mansot, M. Tournoux, J. Power Sources 68 (1997) 698–703.
[25] S.-S. Kim, S. Ogura, H. Ikuta, Y. Uchimoto, M. Wakihara, Solid State Ionics 146 (2002) 249–256.
[26] F. Gillot, M. Ménétrier, E. Bekaert, L. Dupont, M. Morcrette, L. Monconduit, J.-M. Tarascon, J. Power Sources 172 (2007) 877–885.
[27] J. Jamnik, J. Maier, Phys. Chem. Chem. Phys. 5 (2003) 5215–5220.
[28] Y.F. Zhukovskii, P. Balaya, E.A. Kotomin, J. Maier, Phys. Rev. Lett. 96 (2006) 058302.
[29] J. Maier, Faraday Discuss. 134 (2007) 51–66.
[30] J. Maier, J. Power Sources 174 (2007) 569–574.
[31] A. Hightower, C.C. Ahn, B. Fultz, P. Rez, Appl. Phys. Lett. 77 (2002) 238–240.
[32] X.Q. Yang, X. Sun, J. McBreen, Electrochem. Commun. 2 (2000) 100–103.